Gain Curves and Hydrodynamic Simulations of Ignition and Burn for Direct-Drive Fast-Ignition Fusion Targets

Introduction

In fast-ignition[1] inertial confinement fusion (ICF) a cryogenic shell of deuterium and tritium (DT) is first imploded by a high-energy driver to produce an assembly of thermonuclear fuel with high densities and areal densities. Such a dense core is then ignited by the fast electrons (or protons) accelerated through the interaction of a high-power, ultra-intense laser pulse with either a coronal plasma or a solid, cone-shaped target.[2,3] The fast particles slow down in the cold, dense fuel and deposit their kinetic energy through collisions with the background plasma. In direct-drive fast ignition, the high-energy driver is typically a laser with a wavelength $\lambda_L \approx 0.25, 0.35$, or $0.53~\mu$m, and the high-intensity laser has a power in the petawatt range with a wavelength of 0.53 or 1.06 μm. The energy gain is defined as the ratio between the thermonuclear energy yield and the laser energy on target. Such a definition does not take into account the energy required to power the lasers. Including the wall-plug efficiency of the lasers is essential to assess the ultimate validity of fast-ignition inertial confinement fusion as an economical energy source but it requires detailed considerations of the laser technology that are beyond the scope of this article. Earlier attempts[4] to determine the gain curves for fast ignition were based on heuristic models of the fuel assembly and thermonuclear yields. The results shown here represent a calculation of the gain curve based on realistic target designs and hydrodynamic simulations of the implosion, as well as simulations of the ignition by a collimated electron beam and burn propagation. The targets are chosen according to the design of Ref. 5, where the laser pulses and target characteristics are optimized to achieve a fuel assembly with a small hot spot, large densities, and areal densities suitable for fast ignition. Here, we consider a high-energy laser as the compression driver and focus on two forms of the thermonuclear gain. The first is the maximum gain $G_M = E_F / E_c$ given by the ratio between the thermonuclear energy E_F and the compression laser energy on target E_c. The second is the total gain $G_T = E_F / E_T$ defined as the ratio between the thermonuclear energy and the total laser energy on target including the petawatt laser energy $E_T = E_c + E_{pw}$. It is shown in this article that the maximum gain G_M is only a function of the compression laser energy and wavelength $G_M = G_M(E_c, \lambda_L)$, thus leading to the following form of total gain:

$$G_T = \frac{G_M(E_c, \lambda_L)}{1 + E_{pw}/E_c}.\qquad(1)$$

The second term in the denominator of Eq. (1) can be neglected for large compression lasers with $E_c \gg E_{pw}$, thus leading to $G_T \simeq G_M$.

It is important to emphasize that the hydrodynamic simulations of fast-ignition (FI) targets reported in this article are meant to address only one aspect of the physics pertaining to fast ignition: the issue of the hydrodynamic fuel assembly and its potential for high energy gains. The complicated physics of the fast-electron beam generation and transport is not considered here. Instead, the e-beam is assigned as an ideal beam, collimated and uniform, with or without a Maxwellian energy spread. Likely, such an ideal beam is very different from the experimental conditions, where the beam may be broken up into filaments and become divergent. Based on the available experimental data, it is currently not possible to predict the e-beam characteristics in a fast-ignition target because most of the experiments on fast-electron generation and transport pertain to the interaction of intense light with solid targets rather than plasmas relevant to fast ignition.[6] Fast-electron transport properties in plasmas are vastly different than in solid targets,[6] and fast-ignition–relevant plasmas are difficult to produce without an implosion facility. However, the next generation of petawatt lasers such as FIREX-I[7] and OMEGA EP[8] will be combined with an implosion facility and integrated experiments will become possible. Such experiments should provide a wealth of experimental data to be used for the characterization of the fast-electron beam produced in the fast-ignition targets. In this article, the injection of an ideal electron beam is simply assumed. All of the difficulties pertaining to hot-electron generation and transport physics are buried in the parameter describing the conversion efficiency of laser light into collimated hot electrons and the hot-electron temperature.

The latter is either assigned or estimated using the widely used ponderomotive scaling formula,[9] derived from particle-in-cell (PIC) simulations of intense light–plasma interaction. Results based on such a formula should be taken with caution since there is no experimental confirmation that the ponderomotive scaling is applicable to fast-ignition targets. It is also worth mentioning that the conversion efficiency used here defines the conversion of laser light into an ideal collimated beam. Departures from the collimated beam configuration would cause deterioration in efficiency. Because of uncertainties in values of conversion efficiency, the results in this article are parameterized as a function of efficiency.

The hydrodynamic simulations of fast-ignition targets[5] reported in this article include one-dimensional (1-D) simulations of the implosion and two-dimensional (2-D) axisymmetric simulations of ignition by a collimated electron beam and burn propagation. In the case of cone-in-shell targets, the final phase of the implosion is simulated in two dimensions assuming that the cone walls are rigid and truncated at a given distance from the center. This idealized, optimistic configuration is used to estimate the deterioration of the gain due to the presence of the cone. The targets are thick shells of wetted-foam $(DT)_6CH$ with an inner DT-ice layer and a thin CH overcoat. Such targets[5] are designed to achieve a massive compressed core with a uniform density and a small hot spot. Because of their low in-flight aspect ratio (IFAR), such targets are not sensitive to the growth of hydrodynamic instabilities during the acceleration phase. Thus, one-dimensional simulations of the implosions provide a reasonably accurate description of the final fuel assembly (unless a cone is present).

A derivation of the gain curves for target densities around $\rho \approx$ 300 g/cm^3 is described briefly by the same authors in Ref. 10. There, an analytic gain formula is derived and compared with the results of ignition and burn simulations of imploded targets. In Ref. 10, ignition is triggered by a monoenergetic 1- to 3-MeV electron beam with an energy of 15 kJ. The approach used in this article is similar to the one taken by Atzeni in Ref. 11 to describe the ignition conditions for a uniform-density, spherical DT plasma heated by a collimated electron beam. A major step forward in our work is that the DT plasma core is produced by simulating the implosion of realistic fast-ignition targets. Such targets are designed to produce an optimized fuel assembly for fast ignition featuring high densities, high areal densities, and small hot spots. Furthermore, our simulations of ignition and burn are extended to an entire family of fast-ignition targets, scaled for different compression driver energies, to generate a gain curve for direct-drive fast ignition.

This article presents the details of the simulation results that led to the conclusions of Ref. 10. As in Ref. 10, we use a simple parallel straight-line transport model for the fast electrons, in which the electrons lose their energy in the dense core according to the well-established relativistic slowing-down theory of Refs. 12 and 13. Furthermore, we extend the work of Ref. 10 to include sensitivity studies of ignition and gain deterioration due to the cone. The ignition sensitivity studies are carried out with respect to the electron-beam parameters (spot size, duration, electron energy), injection time, fast-electron temporal distribution, and fast-electron distribution function.

To model the energy spectrum of electrons generated by the ultra-intense laser–plasma interaction, simulations using Maxwellian electrons are performed, having ponderomotive temperature scaling with the laser intensity and the wavelength, and assuming a Gaussian temporal profile of the laser pulse. A minimum laser energy for ignition exceeding 100 kJ is found for the 1.054-μm wavelength. Electrons generated by such laser pulses have energies in the range of several MeV. The stopping distance of such energetic electrons in the DT plasma greatly exceeds the optimal for ignition[11] $\rho R = 0.3$ to 1.2, thus increasing the energy required for ignition. The simulations show that the energy of fast electrons, the stopping distance, and the minimum energy for ignition can be reduced using frequency-doubled laser pulses since the mean energy of fast electrons is proportional to the laser wavelength. This conclusion is in agreement with earlier results by Atzeni et al.[14] and Honrubia et al.,[15] where the ponderomotive scaling was used to estimate the fast-electron energy.

In this article, the gain of cone-in-shell targets is also estimated through two-dimensional simulations. Gold cones were suggested as a way to keep a plasma-free path for the fast-ignitor pulses and deliver the petawatt pulse energy to the fuel core. While improving the energy transport to the hot spot, cone-focus geometries can complicate the implosion. A simple model of cone-in-shell targets is considered here, where the shell is imploding along a fixed-boundary "rigid" cone with a truncated tip. After the shell departs from the cone tip, the high-pressure shell plasma is free to expand into the hole left by the cone. This last phase of the implosion is simulated with the two-dimensional hydrocode *DRACO*,[16] which is also used to simulate the ignition and burn phases. This is a highly simplified model of cone-in-shell target implosions, and the resulting gains should be viewed as an optimistic estimate. The simulations show that, in spite of the fact that the shell integrity is not preserved and the density profile is modified facing the cone, the minimum energy for ignition (using monoenergetic

electron beams) is only weakly increased by 3 to 4 kJ, while the target gain is reduced by only 20% to 30%.

The following sections (1) present a summary of the high-density and high-ρR target design recently developed for fast ignition; (2) describes the simulations of ignition and burn using monoenergetic (and Maxwellian) electron beams with prescribed parameters and calculation of the gain curve; (3) discuss the effects of a fast-electron Maxwellian distribution, ponderomotive temperature scaling, and Gaussian laser pulses; and (4) present and discuss the results from simulations of pseudo-cone targets.

Review of the Target Designs and Gain Formula

We follow the work of Ref. 5 with regard to the optimization of the target designs for fast ignition. The optimal fuel assembly for fast ignition[5] requires a small-size, low-temperature hot spot surrounded by a massive cold shell of densities in the 300- to 500-g/cm^3 range. A small and relatively cold hot spot is preferred in that most of the driver energy is used to compress the fuel assembly rather than heating the hot spot. The optimum density for ignition is determined based on considerations concerning the fast-electron energy required for ignition and the fast-electron beam radius. It follows from Atzeni's work[11] that the minimum energy for ignition using a monoenergetic electron beam can be approximated by $E_{ig}^{min} = 11\left[400/\rho(g/cm^3)\right]^{1.85}$ and the optimum beam radius by $r_b^{opt} = 16\left[400/\rho(g/cm^3)\right]^{0.97}$, where ρ is the density of the precompressed DT fuel. While lower ignition energies are needed for greater fuel densities, they require a more-focused electron beam. A reference density of 300 g/cm^3 is often used in the literature, for which a reasonable-sized electron beam of about 20-μm radius requires about 20 kJ of electron energy for ignition. Since technological limitations make it difficult to achieve electron-beam radii shorter than 15 to 20 μm, a fuel density of 300 to 500 g/cm^3 can be a reasonable compromise to keep the ignition energy relatively low without imposing severe requirements on the e-beam focus.

In Ref. 5, relations between the in-flight and stagnation hydrodynamic variables of the imploded shells are derived and used to design optimized fast-ignition targets. According to these relations, the maximum density at stagnation scales as $\rho_{max} \sim V_i/\alpha$ and the maximum areal density scales as $\rho R \sim E_c^{0.33}/\alpha^{0.57}$, where V_i is the implosion velocity at the end of the acceleration phase and α is the value of the in-flight adiabat at the inner shell surface. Here the adiabat is defined as the ratio of the plasma pressure to the Fermi pressure of a degenerate electron gas. For a DT plasma, the adiabat can be approximated by $\alpha \approx p(Mbar)/2.2\,\rho(g/cm^3)^{5/3}$. The aspect ratio at stagnation, defined as the ratio of the hot-spot radius to the shell thickness $A_s = R_h/\Delta_s$, scales as $A_s \sim V_i$. Simple formulas for the target gain and the maximum in-flight aspect ratio (IFAR) are also obtained, according to which $G_M \sim V_i^{-1.25}\theta$ and IFAR $\sim V_i^2/\langle\alpha\rangle^{0.6}$, where $\langle\alpha\rangle$ is the average in-flight adiabat and the common expression for the burn fraction $\theta \approx (1 + 7/\rho R)^{-1}$ can be used. The energy gain decreases with the implosion velocity and increases with ρR. For a given driver energy on target, lower implosion velocities require more massive targets, and therefore more fuel available for reactions. Higher ρR's lead to longer confinement time and therefore higher burn fractions. Thus low implosion velocities (i.e., massive targets) and low adiabats (i.e., high ρR) are necessary to achieve high gains. A low implosion velocity also decreases the IFAR, reducing the growth rate of the most-dangerous Rayleigh–Taylor instability modes. The latter are the Rayleigh–Taylor modes with a wave number k such that $k\Delta_{if} \approx 1$, where Δ_{if} represents the in-flight thickness. Furthermore, with a low implosion velocity, the stagnation aspect ratio, and, consequently, the size and energy of the hot spot, decreases.

The scaling law for the maximum density at stagnation suggests that the minimum implosion velocity is set by the adiabat and the density required for ignition. Thus, high-gain fast-ignition implosions require low values of the inner-surface in-flight adiabat. As long as the ratio $V_i/\alpha \sim \rho$ is sufficiently large to achieve the densities required for fast ignition, the implosion velocity can be minimized by driving the shell on the lowest-possible adiabat. However, very low adiabat implosions require long pulse lengths and careful pulse shaping. The long pulse length is due to the slow velocity of the low-adiabat shocks, and the careful shaping is required to prevent spurious shocks from changing the desired adiabat. Furthermore the ratio between the peak power and the power in the foot of the laser pulse (i.e., the power contrast ratio) increases as the adiabat decreases, thus leading to difficult technical issues in calibrating the pulse shape. These constraints on the pulse shape are alleviated by using the relaxation laser-pulse technique.[17] As suggested in Ref. 5, reasonable minimum values of the inner surface adiabat and implosion velocity are $\alpha \approx 0.7$ and $V_i \sim 1.7 \times 10^7$ cm/s, corresponding to an average density of about 400 g/cm^3. An adiabat below unity implies that at shock breakout, the inner portion of the shell is not fully ionized. Reference 5 also shows that a very modest IFAR $\simeq 16$ corresponds to such implosion velocity and adiabat. Since the number of e foldings for the growth of the most-dangerous Rayleigh–Taylor instability modes with wave number $k \simeq 1/\Delta_{if}$ is approximately $0.9\sqrt{IFAR} \simeq 3.6$, one concludes that the implosion of such capsules is approximately

one dimensional. This is an important consideration since it allows us to make use of the one-dimensional code *LILAC*[18] to simulate the generation of the dense core of the fast-ignition fuel assembly (in the absence of a cone).

It is important to emphasize that the peak values of the density and total areal density occur at different times. As the shell stagnates, the density and areal density grow as a result of the plasma compression induced by the return shock traveling outward from the center. The peak density occurs before the time of peak areal density. Furthermore, a significant amount of relatively low density ($\rho < 200$ g/cm^3), unshocked free-falling plasma surrounds the dense core at the time of peak ρR. Such a low-density plasma carries a significant fraction of the areal density ($\sim 25\%$), thus preventing the fast particles from fully penetrating the dense core. Hence, it can be beneficial to launch the igniter beam soon after the time of peak ρR when the return shock has propagated farther out and compressed the low-density region. One-dimensional simulations of the implosions indicate that at such a time, the average density of the compressed core is about half its peak value.

Using low-velocity implosions of massive shells for fast-ignition fuel assembly should also improve the performance of cone-in-shell targets where a gold cone is inserted into the shell to keep a plasma-free path for the fast-ignitor pulse.[2,3] Recent experiments and simulations of cone-in-shell target implosions[19] have shown that the integrity of the cone tip is compromised by the large hydrodynamic pressures and that a low-density plasma region develops between the cone tip and the dense core, thus complicating the fast-electron transport. Since the stagnation pressure scales as $\rho \sim V_i^{1.8}$ (Ref. 20), the fuel assemblies from low-velocity implosions can improve the cone target's performance since the resulting dense core has relatively low pressure (due to the low velocity), thus reducing the hydrodynamic forces on the cone tip. Furthermore, since low velocities are obtained by imploding shells with large masses, the resulting core size is large, thus reducing the distance between the tip and the dense core edge.

While the simulations in Ref. 5 consider only implosions driven by a compression laser pulse with a wavelength $\lambda = 0.35$ μm, the wavelength dependence for the stagnation variables is included analytically into the gain formula. After setting the values of the adiabat $\alpha \approx 0.7$ and implosion velocity $V_i \sim 1.7 \times 10^7$ cm/s, the maximum gain becomes a function of the compression laser energy and wavelength (see Ref. 10):

$$G_M \approx \frac{743\, I_{15}^{-0.09}\left(0.35/\lambda_L\right)^{0.66}\left(1 - E_{\text{cut}}/E_c\right)^{\mu}}{1 + 21\left(\lambda_L/0.35\right)^{0.25}\Big/\left[\xi E_c^{0.33}\right]} \,, \quad (2)$$

where E_c is in kilojoules and a weak analytical dependence on the maximum pulse intensity $I_{15} \sim 1$ (in units of 10^{15} W/cm^2) is included. This expression uses fitting parameters μ and ξ, which need to be determined by comparison with ignition and burn simulations. Here ξ represents the fraction of the maximum total areal density available for the burn to be used in $\theta(\rho R)\big[\rho R = \xi(\rho R)_{\text{max}}\big]$. The *ad hoc* term $\left(1 - E_{\text{cut}}/E_c\right)^{\mu}$ has been introduced to account for the yield deterioration of small targets where the burn temperature is below 30 keV and the electron-beam size is of the order of the compressed core size occurring for $E_c \sim E_{\text{cut}} \approx 40$ kJ. The factors μ and ξ are of order unity and are to be determined by a numerical fit to the gain in the ignition and burn simulations reported in the next section.

Simulation of Ignition and Burn by Monoenergetic and Maxwellian Electron Beams

To simulate the burn phase of the fast-ignited capsules, we start from the one-dimensional fuel assembly obtained from the code *LILAC* and simulate the ignition by a collimated electron beam and subsequent burn with the two-dimensional, two-fluid hydrocode *DRACO*.[16] The latter has been recently modified[21] to include the electron-beam-energy deposition into the dense fuel. The effects of electron-beam instabilities such as Weibel and resistive filamentation are not included in this work. An overview of the physics issues related to fast-electron generation and transport problem in fast ignition can be found in Refs. 6 and 22. Here a simple straight-line transport model for fast electrons is chosen, in which fast electrons lose energy due to collisions with thermal electrons and to collective plasma oscillations. We use the slowing-down theory of Ref. 13 that includes the effect of multiple scattering. The value of the Coulomb logarithm in the stopping-power term of Ref. 13 has been modified to account for quantum effects. Burn simulations of several fuel assemblies have been performed, characterized by the implosion parameters mentioned above. The targets used in the simulations (Fig. 110.12 shows three of them) are massive wetted-foam targets with an initial aspect ratio of about 2 (outer radius/thickness) driven by UV laser energies varying from 50 kJ to 2 MJ and $I_{15} \simeq 1$. The relaxation-type[17] laser pulses are shown in Fig. 110.13 with the main pulse length varying from 11.5 ns for the 100-kJ target to 22 ns for the 750-kJ target. In all cases, the fast electrons are injected at about 50 μm from the dense core and close to the time of peak areal density.

The main properties of the ignition and burn propagation are illustrated below for a particular example of the 300-kJ fuel assembly. Figure 110.14 shows the target radial density profiles at consecutive moments of time close to the time of maximum areal density. During this period of time, the target expands and the maximum density drops from about 700 g/cm³ to 300 g/cm³. The dense part of the core is surrounded by a relatively low density unshocked region. As the return shock propagates outward, more fuel gets compressed, thus increasing the total ρR available for the burn. Figure 110.15 shows the density (a) as a function of the areal density and (b) as a function of the volume. The areal density of the dense region varies between 1.1 to 1.3 g/cm², while the

ρR in the unshocked region decreases from 0.6 to 0.28 g/cm² with time. The hot-spot volume [Fig. 110.15(b)] is less than 8% of the compressed volume.

Figure 110.16 shows snapshots of ignition and burn simulations for the 300-kJ fuel assembly. Ignition is triggered by a 2-MeV monoenergetic electron beam with a radius of 20 μm and duration of 10 ps. The cylindrically symmetric, radially uniform electron beam is injected from the right. The beam's temporal distribution is also uniform. Ignition is triggered first in a small plasma volume heated by the electrons [Figs. 110.16(a) and 110.16(b)]; the thermonuclear burn wave then propagates to the remaining fuel [Figs. 110.16(c)–110.16(f)].
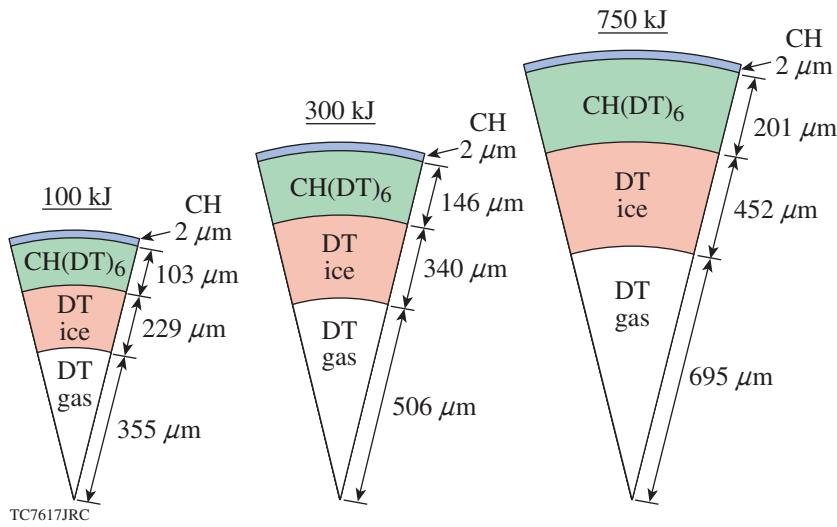

Figure 110.12
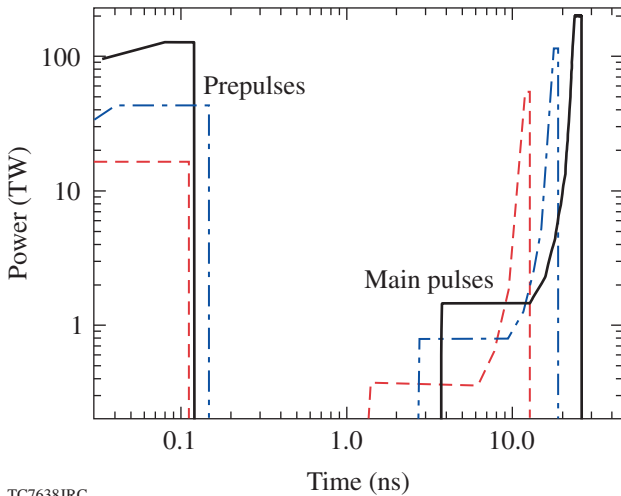100-, 300-, and 750-kJ targets for optimized fast-ignition fuel assembly.

Figure 110.13
Laser pulses (power versus time) for the 100-kJ (dashed lines), 300-kJ (dashed–dotted lines), and 750-kJ (solid lines) targets.
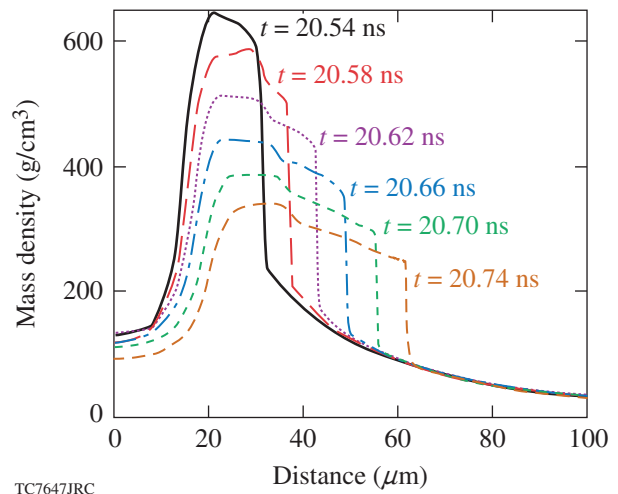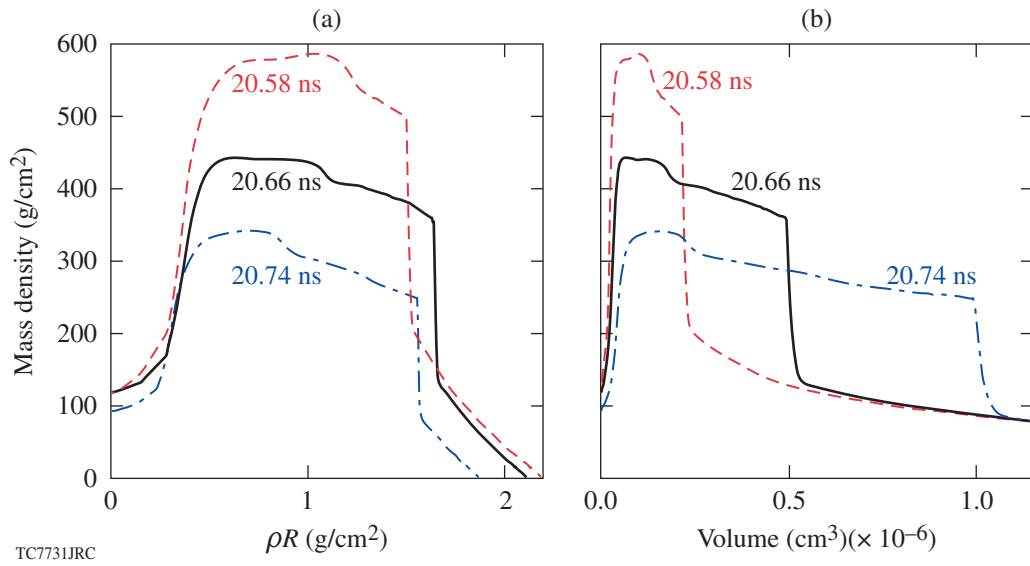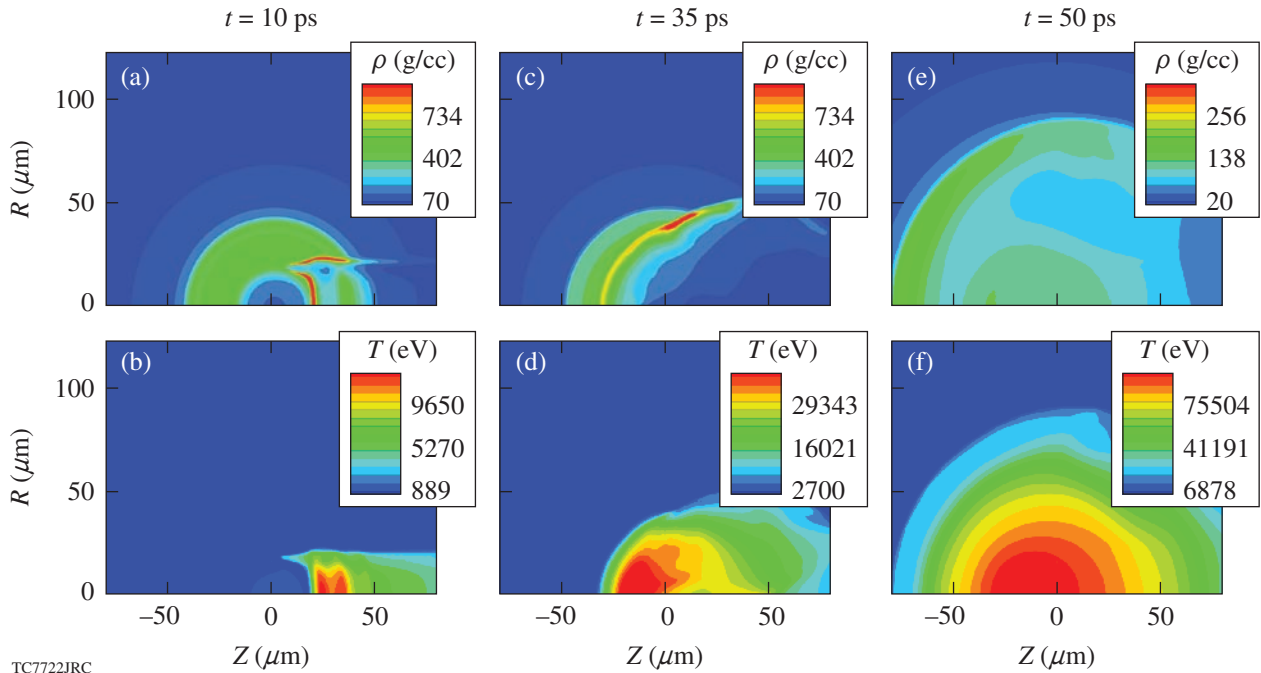

Figure 110.14
Density profiles of the 300-kJ target at different times (about the time of peak ρR) when the fast electrons are injected in the simulations of Fig. 110.17.

TC7731JRC

Figure 110.15
Density profiles of the 300-kJ target versus (a) areal density and (b) volume at three times near the time of peak ρR.

TC7722JRC

Figure 110.16
Contour plots of the density (ρ) and ion temperature (T) at selected moments of time in the burn simulation induced by ignition by an 18-kJ, 10-ps, 2-MeV monoenergetic electron beam.

We have performed simulations using monoenergetic electron beams to find how the minimum energy for ignition depends on the electron-beam parameters and the injection time. The results for the 300-kJ fuel assembly are shown below. Figure 110.17 shows the dependence of the minimum ignition energy for a 10-ps, 2-MeV monoenergetic electron beam on the beam injection time for three beam radii: 20, 30, and 40 μm. The minimum ignition energy is found with an error ≤4% by changing the total electron-beam energy while keeping all the other parameters constant. For a 20-μm electron beam, minimum ignition energy of about 15 kJ is found when the density is maximum for earlier injection times. It increases for late injections when the target density decreases. While focused beams with a radius ≤20 μm are preferable for ignition, realistic electron beams may have a larger spot size when entering the fuel core because of their angular spread. For a 30-μm electron beam, the ignition energy reaches its minimum of 26 kJ at the injection time of $t = 20.58$ ns and for a 40-μm beam the minimum ignition energy is 41 kJ at $t = 20.62$ ns.

Atzeni's formula can be attributed to the loss of fast electrons in the low-density unshocked region. Notice that the electron-pulse duration in our simulation is less than the hydrodynamic confinement time of the heated region as required by Atzeni.

Figure 110.18(a) shows the dependence of the minimum ignition energy on the beam radius for a pulse duration of 10 ps and injection time of 20.62 ns. Figure 110.18(b) shows how the minimum ignition energy depends on the electron-pulse duration for a fixed radius of 20 μm and the same injection time. The minimum ignition energy increases with both the electron-beam radius and pulse duration.

Figure 110.19 shows the dependence of the minimum ignition energy on the electron energy. The beam radius is 20 μm, the pulse duration is 10 ps, and the injection time is 20.62 ns.
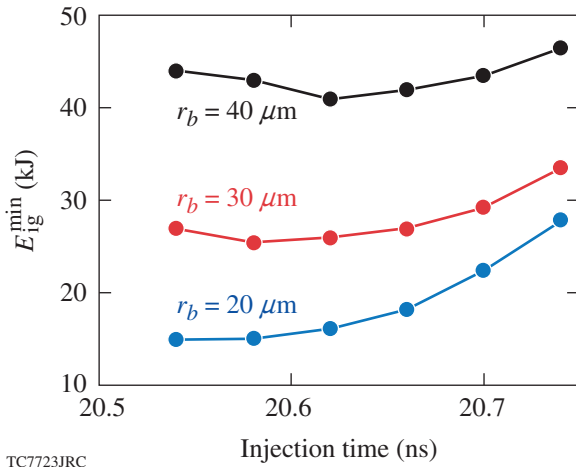

TC7723JRC

Figure 110.17
Minimum ignition energy versus injection time for a 10-ps, 2-MeV monoenergetic electron beam and three values of the beam radius: 20, 30, and 40 μm.

The minimum energy for ignition found in our simulations is in good agreement with that found by Atzeni.[11] According to Atzeni's formula, the minimum ignition energy of 19.7 kJ is reached for a density of 300 g/cm^3 and a beam radius of 20 μm. Our simulations predict a minimum ignition energy of about 25 kJ for the same beam radius and injection when the density has a similar value in the dense region. The 25% difference in the ignition energy between our simulations and
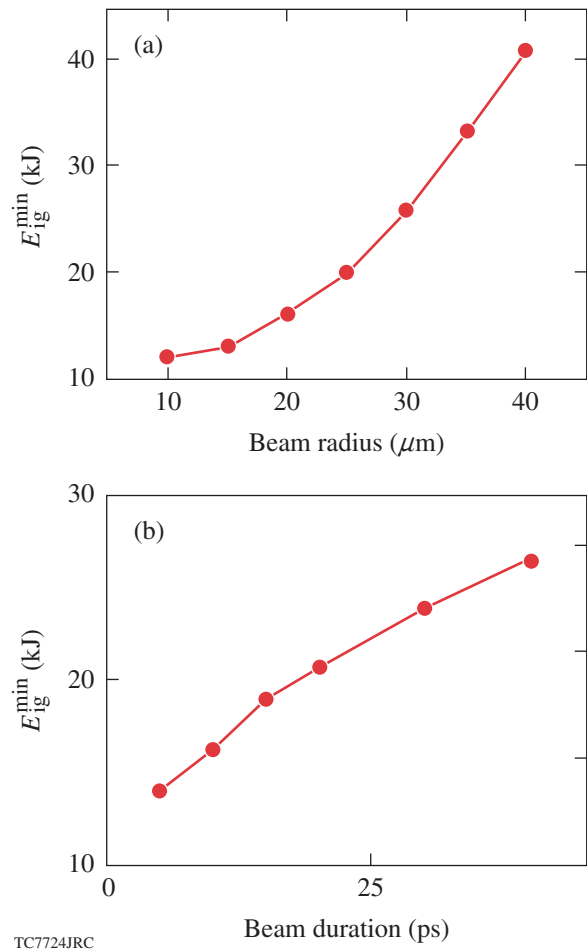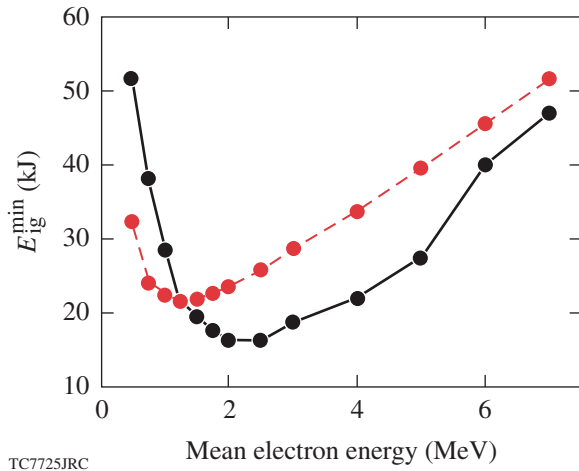

TC7724JRC

Figure 110.18
Minimum ignition energy versus (a) beam radius and (b) duration for a 2-MeV monoenergetic electron beam. (a) The beam duration is 10 ps and (b) the beam radius is 20 μm.

The results for monoenergetic electrons (solid line) and electrons with an energy spread (dashed line) are shown. In the simulations with an energy spread, a relativistic Maxwellian electron distribution function is used. For monoenergetic electrons, the lowest ignition energy of 16.25 kJ is reached at 2 MeV, while for Maxwellian electrons, 21.5 kJ for the mean energy of 1.25 MeV is reached. The minimum ignition energy is higher for Maxwellian electrons because the energy is deposited over a larger region in the longitudinal direction and is not as localized as for monoenergetic electrons. This is seen from the snapshots for the plasma temperature just after the energy is deposited by fast electrons ($t = 10$ ps) in the simulations with 2-MeV Maxwellian (Fig. 110.20) and monoenergetic electrons (Fig. 110.16). Maxwellian electrons with $E > \langle E \rangle$ transfer more energy than electrons with $E < \langle E \rangle$. This explains why the mean electron energy that minimizes the ignition energy is lower for Maxwellian than for monoenergetic electrons. Figure 110.19 also shows that the minimum ignition energy greatly increases for high-energy multi-MeV electrons. This is because the stopping length of such electrons greatly exceeds the optimal size of the heated region[11] $0.3 < \rho R < 1.2$ g/cm^2, so that a much longer region is heated. Unfortunately, this appears to be the case of realistic laser pulses (see **Simulation of Ignition by Maxwellian Electrons with Ponderomotive Temperature Scaling and Gaussian Laser Pulses**, p. 82).

Our simulations for different targets show that, for a 20-μm beam radius, the minimum energy required for ignition is consistently $\approx$15 kJ using electron beams with a 20-μm radius.

As long as the ignition is triggered, the thermonuclear energy yield is approximately independent of the electron-beam characteristics. The neutron yields for the 100-, 300-, and 750-kJ assemblies are 2.0×10^{18}, 1.2×10^{19}, and 4.2×10^{19}, and the thermonuclear energy yields are 5.6, 34, and 118 MJ, respectively. The results of these simulations are used to determine the fitting parameters $\xi \approx 0.7$ and $\mu \approx 1.1$ in Eq. (2), leading to the following maximum gain formula:

$$G_M = \frac{743\, I_{15}^{-0.09}\left(0.35/\lambda_L\right)^{0.66}\left(1 - E_{\text{cut}}/E_c\right)^{1.1}}{1 + 30\left(\lambda_L/0.35\right)^{0.25}/E_c^{0.33}}, \quad (3)$$

where E_c is in kilojoules and $E_{\text{cut}} \approx 40$ kJ. Notice that even a modest-sized UV laser driver with an energy of 100 kJ can produce a fuel assembly yielding a maximum gain close to 60. Figure 110.21 shows that Eq. (3) accurately fits all simulation results and can be used to determine the total gain in Eq. (1). Figure 110.22 shows the total gain for three values of the ignition-pulse energy $E_{\text{PW}} = 50$ kJ, 75 kJ, and 150 kJ. Even in the case of $E_{\text{PW}} = 150$ kJ, the target gain from a 100-kJ fuel assembly is still remarkably high ($G_T \simeq 22$).
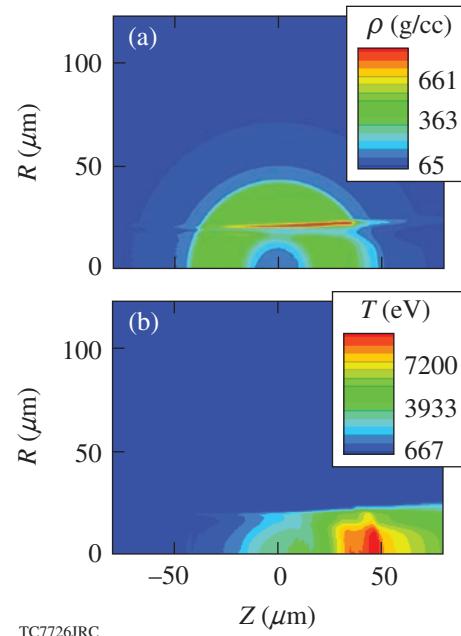

TC7725JRC

Figure 110.19
Minimum ignition energy versus electron energy for 2-MeV monoenergetic (solid line) and Maxwellian (dashed line) electron beams. The beam duration is 10 ps and the radius is 20 μm.

TC7726JRC

Figure 110.20
Contour plots of the density and ion temperature after the 300-kJ target is heated by a 25-kJ, 10-ps, 20-μm, 2-MeV Maxwellian electron beam.
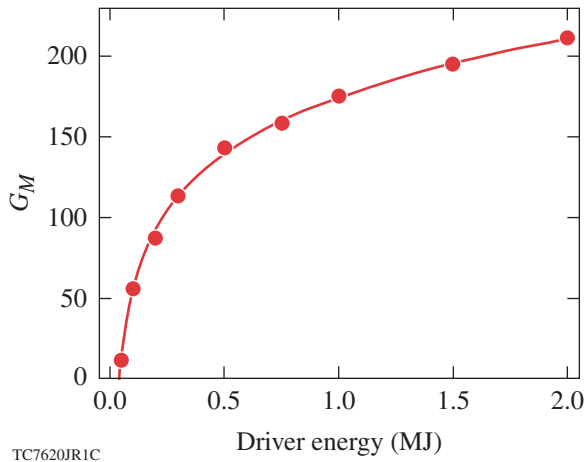
Figure 110.21
Maximum gain (energy yield/compression driver energy) versus compression driver energy from Eq. (3) (curve) and *DRACO* simulations (dots).
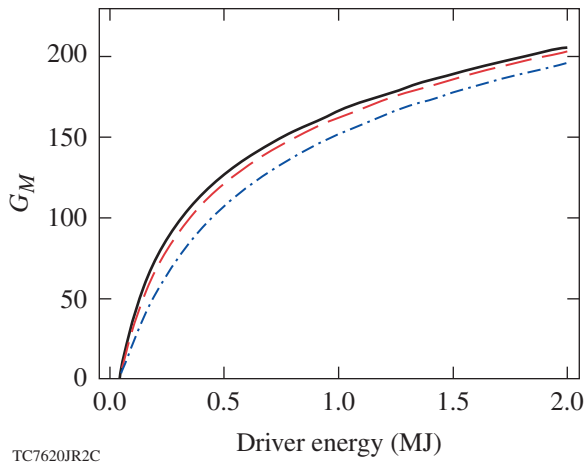

Figure 110.22
Target gain (energy yield/total energy on target) versus compression driver energy for E_{PW} = 50 kJ (solid line), 75 kJ (dashed line), and 150 kJ (dashed–dotted line).

**Simulation of Ignition by Maxwellian Electrons
with Ponderomotive Temperature Scaling
and Gaussian Laser Pulses**

Hot electrons in fast ignition are produced during the interaction of ultra-intense laser pulses with either the coronal plasma or a solid target. The spectrum of fast electrons and the energy conversion efficiency from the laser to electrons generally depend on the details of this interaction. An assumption, however, is often used[14,15,23] that the mean energy of hot electrons equals the energy of their oscillation in the laser field $E \sim mc^2 (\gamma-1)$ (so-called ponderomotive scaling[9]), where

$\gamma = \sqrt{1 + p^2/2}$, $p \sim eA/mc^2$ is the momentum of electrons (normalized to mc) in the linearly polarized laser field with the amplitude of the vector potential A. The experimental data predict different values of the energy conversion efficiency from the laser to electrons in the range $\eta \sim 0.2$ to 0.5 for laser intensities $I > 10^{19}$ W/cm^2 (Refs. 2 and 24). We have performed simulations assuming a Gaussian temporal profile for the laser pulse and a relativistic Maxwellian distribution function for fast electrons with a mean energy following the ponderomotive scaling that can also be rewritten as

$$\langle E \rangle \approx \left[\frac{I(\lambda/1.054 \ \mu m)^2}{10^{19} \ W/cm^2} \right]^{1/2} \ MeV. \qquad (4)$$

According to this scaling, the mean energy is a function of the laser intensity and the wavelength. Notice that for a relativistic Maxwellian distribution function of the form $f(E) \sim \exp[-mc^2(\gamma - 1)/kT](\gamma^2 - 1)^{1/2}\gamma$, the mean energy is $\langle E \rangle = 3kT/2$ in the nonrelativistic and $\langle E \rangle = 3kT$ in the ultra-relativistic limit. Two values of the energy conversion efficiency to fast electrons were used: $\eta = 0.3$ and $\eta = 0.5$. Simulations with different parameters of the laser pulse such as spot size (rectangular beam profile in the radial direction), duration, and wavelengths of 1.054 μm and 0.527 μm were performed for the 300-kJ fuel assembly to find the minimum energy required for ignition. The optimal injection time is found to be close to $t = 20.62$ ns when the averaged density is about 450 g/cm^3. Using a smaller beam radius and pulse duration lead to higher intensities and more-energetic electrons, according to the ponderomotive scaling Eq. (4). However, very energetic (multi-MeV) electrons require a large stopping distance that can even exceed the size of small-to-moderate energy targets. Larger beam radii with $\rho r_b > 0.6$ g/cm^2 lead to a heated volume greater than the optimal value.[11] Also very long laser pulses with durations exceeding the confinement time of the heated region are detrimental and lead to a higher ignition energy. Optimal values of the duration and radius exist for which the laser ignition energy is minimized.

A set of simulations was performed to find such conditions. Tables 110.I and 110.II summarize the results. The optimal laser pulse duration and radius, the mean hot-electron energy (at the time of the Gaussian peak), the electron-beam fuel coupling efficiency, and the minimum ignition energy (of the laser pulse and the electron beam) are provided from simulations carried out with two values of the coupling efficiency and two laser wavelengths ($\lambda = 1.054 \ \mu m$ and 0.527 μm). The minimum laser energy for ignition is 235 kJ (with 71 kJ in fast electrons) for

Table 110.I: Summary of the simulations for $\lambda = 1.054$ μm.

η	r_b (μm)	τ_b (ps)	$E_{\text{las.ig}}^{\min}$ (kJ)	$E_{\text{e.ig}}^{\min}$ (kJ)	$\langle E \rangle$ (MeV)	$\eta_{e-\text{pl}}$
0.3	26.3	16.3	235	71	7.7	0.69
0.5	22.5	13.8	105	53	6.3	0.76

Table 110.II: Summary of the simulations for $\lambda = 0.527$ μm.

η	r_b (μm)	τ_b (ps)	$E_{\text{las.ig}}^{\min}$ (kJ)	$E_{\text{e.ig}}^{\min}$ (kJ)	$\langle E \rangle$ (MeV)	$\eta_{e-\text{pl}}$
0.3	19	8	106	32	3.7	0.86
0.5	16.8	7	50	25	3.2	0.92

wavelength $\lambda = 1.054$ μm and conversion efficiency $\eta = 0.3$ (Table 110.I). Figure 110.23 shows snapshots of the plasma density and ion temperature for this simulation at two moments of time: at the end of the laser pulse and at the developed burn stage. Figure 110.23(b) shows that the plasma is heated throughout the core. Electrons are not completely stopped in the core and continue to heat the low-density plasma behind it. Ignition is triggered first in the plasma column heated by the electrons and the burn region then expands radially [Figs. 110.23(c) and 110.23(d)]. The laser intensity at the time of the Gaussian peak is 6.5×10^{20} W/cm^2, and very energetic electrons are

produced with a mean energy of 7.7 MeV (Table 110.I). Only 69% of the total electron energy is deposited into the plasma. Table 110.I also shows that the laser energy required for ignition decreases to 105 kJ (53 kJ in fast electrons) for $\eta = 0.5$. This significant reduction in the ignition energy is due not only to a larger fraction of the laser energy converted into hot electrons but also to the lower electron energies produced with reduced intensities.

It was suggested by Atzeni and Tabak[14] that shorter laser wavelengths can reduce the mean energy of fast electrons [see Eq. (4)], their stopping length, and the energy required for ignition. Indeed, Table 110.II shows that for a frequency-doubled green light ($\lambda = 0.527$ μm), the laser energy required for ignition decreases to 106 kJ (32 kJ in fast electrons) for $\eta = 0.3$ and 50 kJ (25 kJ in fast electrons) for $\eta = 0.5$. The mean hot-electron energy, however, is still high in these simulations (3.7 MeV and 3.2 MeV, respectively), which suggests that even shorter laser wavelengths can be desirable.

While simulations predict that using a green laser light reduces the energy required for ignition, frequency doubling of the red light with high conversion efficiency can present a technologically challenging task. In this context, finding other mechanisms to reduce the energy of hot electrons generated by ultra-intense laser pulses would be very helpful.
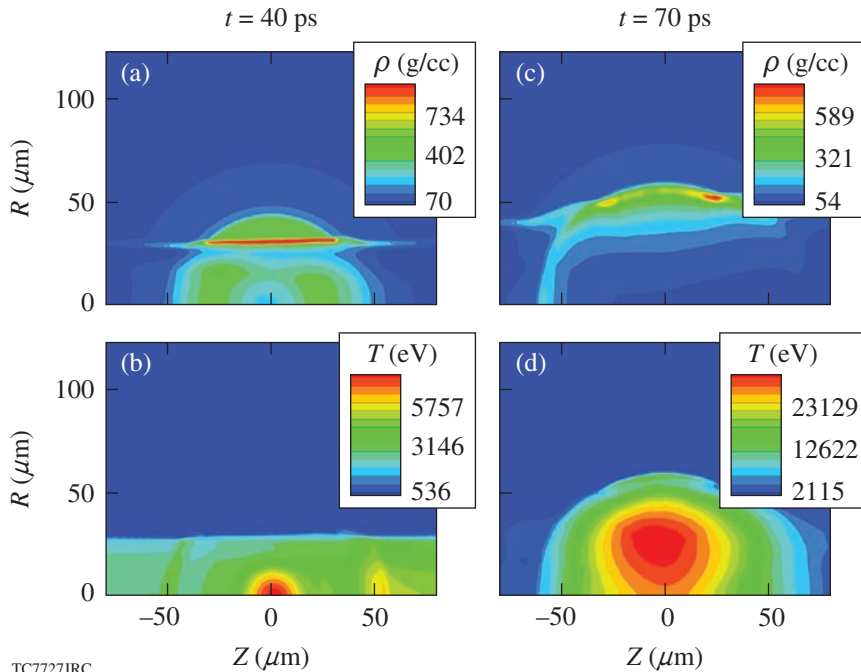

Figure 110.23
Contour plots of the density and ion temperature at selected moments of time in the burn simulation induced by a 235-kJ, 26.3-μm, 16.3-ps laser pulse with an energy conversion efficiency to fast electrons of $\eta = 0.3$.

TC7727JRC

Simulations of Pseudo-Cone Targets

The use of gold cones is currently considered as one of the most promising options to deliver the petawatt-pulse laser energy to the compressed fuel. The cone provides an access path for an ignition laser beam to the fuel, free of the coronal plasma that otherwise can reflect the laser light at the critical plasma surface 1 to 2 mm away from the compressed core. Fast electrons are produced by the interaction of the laser beam with the cone tip located tens to a few hundred microns from target center and then transported toward the core. Cone-focus geometries, while improving the transport of energy to the hot spot, can complicate the implosion. The question arises whether the fuel can still be compressed to the same high densities and areal densities as for spherically symmetric implosions. The compressed core should be significantly modified from the side of the cone where the laser-generated fast electrons enter the core to ignite it. It is important to determine how the minimum energy for ignition and the target gain are affected by the cone.

We have performed simulations of cone-target implosions using a highly simplified model of the cone. We assume that the cone walls are rigid and truncated at a given distance from the center. The pseudo-cone target is schematically shown in Fig. 110.24. The cone walls are directed toward the center of the target and truncated at a distance of about 200 μm from it. The cone opening angle is 90°. A narrow cone tip may exist and go farther toward the center. We use 1-D *LILAC* implo-

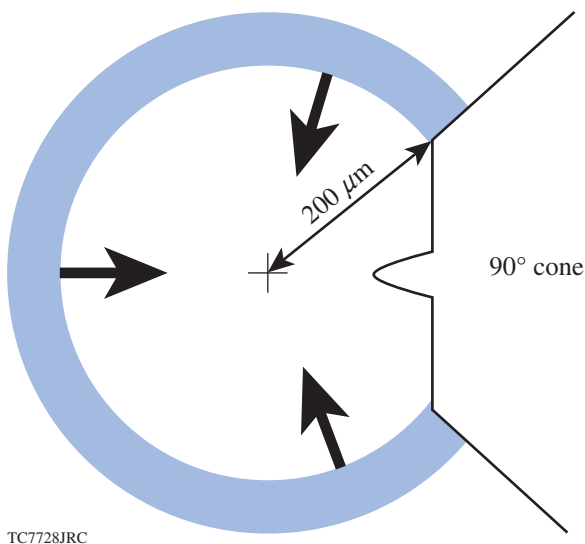sion simulations until the converging shell reaches the cone tip. From this point on, the simulation is continued with the 2-D *DRACO* code. The 1-D *LILAC* outputs are used as initial conditions (time $t = 0$) after removing the section of the shell corresponding to the cone tip. Such a model accounts only for the effect associated with the hole left in the shell after its departure from the cone. Other effects such as shear flow down the sides of the cone and DT contamination by the gold[19,25] or more-complicated cone shapes are not considered here and will be addressed in future work.

We first study how the perturbed shell converges. Figure 110.25 shows snapshots of the fuel density in the *DRACO* simulation for the 300-kJ fuel assembly. The 2-D simulation starts from the spherically symmetric shell with the hole caused by the cone. When the shell approaches the center, the hole does not close and the hot gas flows out from the central region. Figure 110.25(c) shows the density profile at the moment of time ($t = 0.98$ ns) when the maximum density is reached in the simulation without the cone, while Fig. 110.25(d) covers the moment of time ($t = 1.14$ ns) slightly before the maximum areal density. At $t = 0.98$ ns, the density profile on the left side of the target is practically the same as in the 1-D simulation (without the cone) and the maximum density is approximately the same. At $t = 1.14$ ns, the density profile on the left side is still close to that in the 1-D simulation except for the hot spot, which shrinks. The opening in the shell at $t = 1.14$ ns has a radius of about 6 μm and is surrounded by a high-density region. While the compressed core is certainly modified by the cone, these changes do not seem to significantly affect the ignition energy requirements. To verify this, we have performed burn simulations using a 2-MeV monoenergetic electron beam with a radius of 20 μm and a duration of 10 ps, injected at $t = 1.14$ ns in the z direction. It is found that the ignition energy increased by only 4 kJ to 19 kJ with respect to the 1-D implosion without the cone. The maximum gain in the pseudo-cone target simulation is equal to 90 instead of 113 without the cone.

Similar pseudo-cone simulations were performed for other targets driven by laser pulses with energies ranging from 50 kJ to 2 MJ. For all of the targets, the minimum ignition energy ranges from 18 to 20 kJ and is found to be only weakly affected by the cone. Figure 110.26 shows the maximum gain in the pseudo-cone target simulations and the gain predicted by Eq. (3). The maximum gain decreases by 20% to 25% for driver pulse energy between 200 kJ and 2000 kJ and slightly more (up to 30%) for lower-energy drivers. Notice that removing a part of the shell in place of the cone in these simulations reduces the total mass of the thermonuclear fuel by approximately 15%;
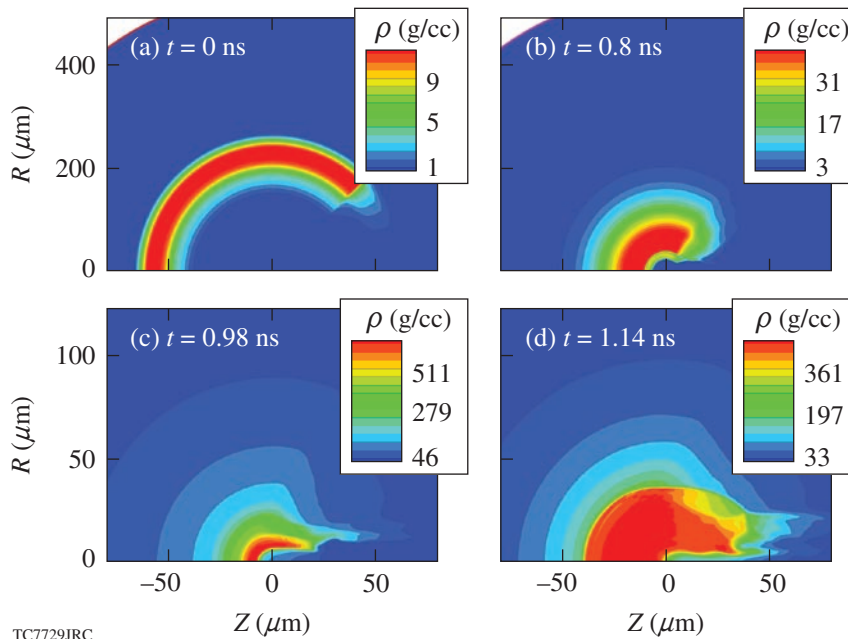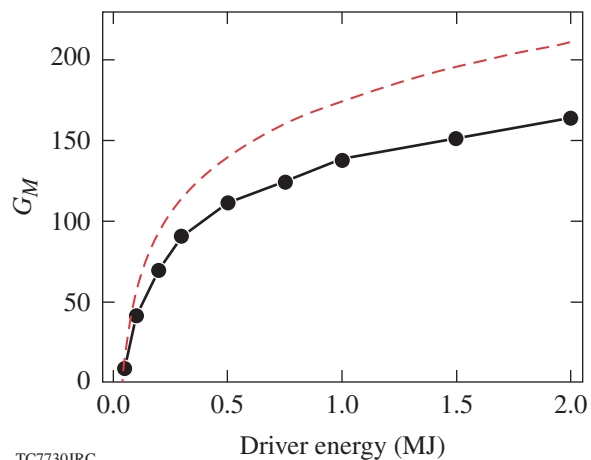

TC7728JRC

Figure 110.24
Pseudo-cone target.

Figure 110.25
Contour plots of the density at different times in the pseudo-cone-target simulation.

Figure 110.26
Maximum gain versus compression driver energy for the pseudo-cone targets (dots connected by a solid line) and for spherically symmetric implosions [Eq. (3)] (dashed line).

however, the maximum gain in the simulation is reduced more than that. This signifies that not all of the remaining fuel can be assembled so effectively as for an unperturbed shell. Nevertheless, the reduced gain in the pseudo-cone target simulations is still remarkably high; in particular, a maximum gain of 70 is still possible with driver-pulse energies of only 200 kJ.

Summary and Discussion

Hydrodynamic simulations of realistic, high-gain, fast-ignition targets, including one-dimensional simulations of the implosion and two-dimensional simulations of ignition by a collimated electron beam and burn propagation are presented and discussed in this article. The targets' design is based on the fuel assembly theory of Ref. 5. The fast-ignition targets are massive wetted-foam, cryogenic DT shells with an initial aspect ratio close to 2. They are imploded by relaxation-type pulses to form high-density and high-areal-density cores with small hot spots, which are optimal for fast ignition. Due to the large thickness and small in-flight aspect ratio, such targets are practically unperturbed by Rayleigh–Taylor instability, making 1-D hydrocodes suitable to simulate the implosion.

The simulations of ignition and burn have been used to find the minimum energy for ignition and to generate gain curves for direct-drive, fast-ignition inertial confinement fusion based on realistic fast-ignition target designs. A large number of runs for targets driven by UV-laser compression pulses with energies from 50 kJ to 2 MJ have been performed. Fitting parameters in the analytical scaling for the target gain are obtained, accounting for the fraction of the maximum total areal density available for the burn and yield deterioration of small targets. It is found that even modest-sized UV-laser drivers, with an energy of 100 kJ, can produce a fuel assembly yielding a maximum gain (energy yield/compression driver energy) close to 60. Assuming a 100-kJ ignition laser pulse, the total gain (energy yield/total energy on target) can be as high as 30 for a 100-kJ compression pulse and about 60 for a 200-kJ driver. Notice that at 1 MJ, the total gain of the optimized fast-ignition target $G_T = 160$ (for a 100-kJ ignition pulse) is considerably higher than the gain of

direct-drive NIF targets, $G \simeq 50$ (Ref. 26). Although less than earlier heuristic model predictions[4] (which also use different optimizations), Eq. (3) shows that fast ignition can achieve significant gains with relatively small drivers.

In our simulations of ignition and burn, the energy of fast electrons, beam radius (20 μm and larger), and pulse length were varied to find the minimum beam energy for ignition close to 15 kJ for different (25-kJ to 2-MJ driver-pulse energy) fuel assemblies, using monoenergetic electron beams. The dependence of the minimum beam energy for ignition on the electron-beam parameters and injection time has been analyzed in detail. The minimum beam energy for ignition increases up to 20 kJ for electrons with energy spread (relativistic Maxwellian distribution function) and optimal mean energy. Simulations using ponderomotive temperature scaling for fast electrons with the laser intensity and Gaussian (in time) laser pulses have also been performed for the 300-kJ fuel assembly. It is shown that for a laser wavelength of 1.054 μm, the minimum laser pulse energy required for ignition is 235 kJ (with 71 kJ in fast electrons) if the energy conversion efficiency from the laser to fast electrons is 30%. The laser ignition energy decreases to 105 kJ (53 kJ in fast electrons) if the energy conversion efficiency is 50%. Such large laser ignition energies are caused by the high electron energy. Indeed, the hot electrons produced by ultra-intense laser pulses have multi-MeV energies, and their stopping range can greatly exceed the optimal value for fast ignition. A possible solution may be using frequency-doubled ignition pulses, for which the mean energy of fast electrons decreases by a factor of 2 (for the same laser intensity). Simulations for a laser wavelength of 0.527 μm predict a minimum laser pulse energy for ignition of 106 kJ (with 32 kJ in fast electrons) for an energy conversion efficiency of 30% and 50 kJ (25 kJ in fast electrons) for a conversion efficiency of 50%. It has been reported[27] that sharp solid–plasma interface electrons can be produced with energy below the ponderomotive scaling prediction. A strong reduction in energy conversion efficiency to fast electrons, however, simultaneously takes place. Finding mechanisms to reduce the energy of fast electrons without a significant loss of conversion efficiency would be very helpful to avoid a technologically complicated task of resorting to green laser light for high-power lasers.

We have also performed simplified cone-target simulations assuming that the cone walls are rigid and truncated at a certain distance from the center. Such simulations predict a gain deterioration of 20% to 30% and a small increase in the minimum ignition energy with respect to unperturbed targets. More-sophisticated cone models are currently under

implementation in the code *DRACO*[28] and the results from more-realistic cone-in-shell target implosion simulations will be reported in future articles.

ACKNOWLEDGMENT

REFERENCES

1. M. Tabak *et al.*, Phys. Plasmas **1**, 1626 (1994).

2. R. Kodama *et al.*, Nature **412**, 798 (2001).

3. K. A. Tanaka *et al.*, Phys. Plasmas **10**, 1925 (2003); P. A. Norreys, K. L. Lancaster, C. D. Murphy, H. Habara, S. Karsch, R. J. Clarke, J. Collier, R. Heathcote, C. Hernandez-Gomez, S. Hawkes, D. Neely, M. H. R. Hutchinson, R. G. Evans, M. Borchesi, L. Romagnani, M. Zepf, K. Akli, J. A. King, B. Zhang, R. R. Freeman, A. J. MacKinnion, S. P. Hatchett, P. Patel, R. Snavely, M. H. Key, A. Nikroo, R. Stephens, C. Stoeckl, K. A. Tanaka, T. Norimatsu, Y. Toyama, and R. Kodama, Phys. Plasmas **11**, 2746 (2004).

4. M. Tabak *et al.*, Fusion Sci. Technol. **49**, 254 (2006).

5. R. Betti and C. Zhou, Phys. Plasmas **12**, 110702 (2005).

6. R. R. Freeman *et al.*, Fusion Sci. Technol. **49**, 297 (2006); R. R. Freeman, K. Akli, F. Beg, R. Betti, S. Chen, D. J. Clark, P. M. Gu, G. Gregori, S. P. Hatchett, D. Hey, K. Highbarger, J. M. Hill, N. Izumi, M. Key, J. A. King, J. A. Koch, B. Lasinki, B. Langdon, A. J. MacKinnon, D. Meyerhofer, N. Patel, P. Patel, J. Pasley, H. S. Park, C. Ren, R. A. Snavely, R. B. Stephens, C. Stoeckl, M. Tabak, R. Town, L. Van Woerkom, R. Weber, S. C. Wilks, and B. B. Zhang, J. Phys. IV France **133**, 95 (2006); M. Tabak *et al.*, Phys. Plasmas **12**, 057305 (2005); R. B. Stephens, R. P. J. Snavely, Y. Aglitskii, K. U. Akli, F. Amiranoff, C. Andersen, D. Batani, S. D. Baton, T. Cowan, R. R. Freeman, J. S. Green, H. Habara, T. Hall, S. P. Hatchett, D. S. Hey, J. M. Hill, J. L. Kaae, M. H. Key, J. A. King, J. A. Koch, R. Kodama, M. Koenig, K. Krushelnick, K. L. Lancaster, A. J. MacKinnon, E. Martinolli, C. D. Murphy, M. Nakatsutsumi, P. Norreys, E. Perelli-Cippo, M. Rabec Le Gloahec, B. Remington, C. Rousseaux, J. J. Santos, F. Scianitti, C. Stoeckl, M. Tabak, K. A. Tanaka, W. Theobald, R. Town, T. Yabuuchi, and B. Zhang, J. Phys. IV France **133**, 355 (2006).

7. K. Mima, T. Takeda, and FIREX Project Group, Fusion Sci. Technol. **49**, 358 (2006).

8. C. Stoeckl, J. A. Delettrez, J. H. Kelly, T. J. Kessler, B. E. Kruschwitz, S. J. Loucks, R. L. McCrory, D. D. Meyerhofer, D. N. Maywar, S. F. B. Morse, J. Myatt, A. L. Rigatti, L. J. Waxer, J. D. Zuegel, and R. B. Stephens, Fusion Sci. Technol. **49**, 367 (2006).

9. S. C. Wilks *et al.*, Phys. Rev. Lett. **69**, 1383 (1992).

10. R. Betti, A. A. Solodov, J. A. Delettrez, and C. Zhou, Phys. Plasmas **13**, 100703 (2006).

11. S. Atzeni, Phys. Plasmas **6**, 3316 (1999).

12. C. Deutsch *et al.*, Phys. Rev. Lett. **77**, 2483 (1996).

13. C. K. Li and R. D. Petrasso, Phys. Rev. E **70**, 067401 (2004).

14. S. Atzeni and M. Tabak, Plasma Phys. Control. Fusion **47**, B769 (2005).

15. J. J. Honrubia and J. Meyer-ter-Vehn, Nucl. Fusion **46**, L25 (2006).

16. P. B. Radha, T. J. B. Collins, J. A. Delettrez, Y. Elbaz, R. Epstein, V. Yu. Glebov, V. N. Goncharov, R. L. Keck, J. P. Knauer, J. A. Marozas, F. J. Marshall, R. L. McCrory, P. W. McKenty, D. D. Meyerhofer, S. P. Regan, T. C. Sangster, W. Seka, D. Shvarts, S. Skupsky, Y. Srebro, and C. Stoeckl, Phys. Plasmas **12**, 056307 (2005).

17. R. Betti, K. Anderson, J. Knauer, T. J. B. Collins, R. L. McCrory, P. W. McKenty, and S. Skupsky, Phys. Plasmas **12**, 042703 (2005).

18. J. Delettrez, R. Epstein, M. C. Richardson, P. A. Jaanimagi, and B. L. Henke, Phys. Rev. A **36**, 3926 (1987).

19. R. B. Stephens *et al.*, Phys. Rev. Lett. **91**, 185001 (2003); R. B. Stephens, S. P. Hatchett, M. Tabak, C. Stoeckl, H. Shiraga, S. Fujioka, M. Bonino, A. Nikroo, R. Petrasso, T. C. Sangster, J. Smith, and K. A. Tanaka, Phys. Plasmas **12**, 056312 (2005).

20. C. D. Zhou and R. Betti, "Hydrodynamic Relations for Direct-Drive Fast-Ignition and Conventional Inertial Confinement Fusion Implosions," submitted to Physics of Plasmas.

21. J. A. Delettrez, J. Myatt, P. B. Radha, C. Stoeckl, S. Skupsky, and D. D. Meyerhofer, Plasma Phys. Control. Fusion **47**, B791 (2005).

22. Y. Sentoku *et al.*, Fusion Sci. Technol. **49**, 278 (2006).

23. R. P. J. Town *et al.*, Nucl. Instrum. Methods Phys. Res. A **544**, 61 (2005); R. J. Mason, Phys. Rev. Lett. **96**, 035001 (2006).

24. M. H. Key *et al.*, Phys. Plasmas **5**, 1966 (1998); R. Kodama *et al.*, Nature **418**, 933 (2002); K. Yasuike *et al.*, Rev. Sci. Instrum. **72**, 1236 (2001); M. H. Key, M. D. Cable, T. E. Cowan, K. G. Estabrook, B. A. Hammel, S. P. Hatchett, E. A. Henry, D. E. Hinkel, J. D. Kilkenny, J. A. Koch, W. L. Kruer, A. B. Langdon, B. F. Lasinski, R. W. Lee, B. J. MacGowan, A. MacKinnon, J. D. Moody, M. J. Moran, A. A. Offenberger, D. M. Pennington, M. D. Perry, T. J. Phillips, T. C. Sangster, M. S. Singh, M. A. Stoyer, M. Tabak, G. L. Tietbohl, M. Tsukamoto, K. Wharton, and S. C. Wilks, Phys. Plasmas **5**, 1966 (1998).

25. S. P. Hatchett, D. Clark, M. Tabak, R. E. Turner, C. Stoeckl, R. B. Stephens, H. Shiraga, and K. Tanaka, Fusion Sci. Technol. **49**, 327 (2006).

26. P. W. McKenty, V. N. Goncharov, R. P. J. Town, S. Skupsky, R. Betti, and R. L. McCrory, Phys. Plasmas **8**, 2315 (2001).

27. S. C. Wilks and W. L. Kruer, IEEE J. Quantum Electron. **33**, 1954 (1997).

28. K. S. Anderson, R. Betti, P. W. McKenty, P. B. Radha, and M. M. Marinak, Bull. Am. Phys. Soc. **51**, 32 (2006).